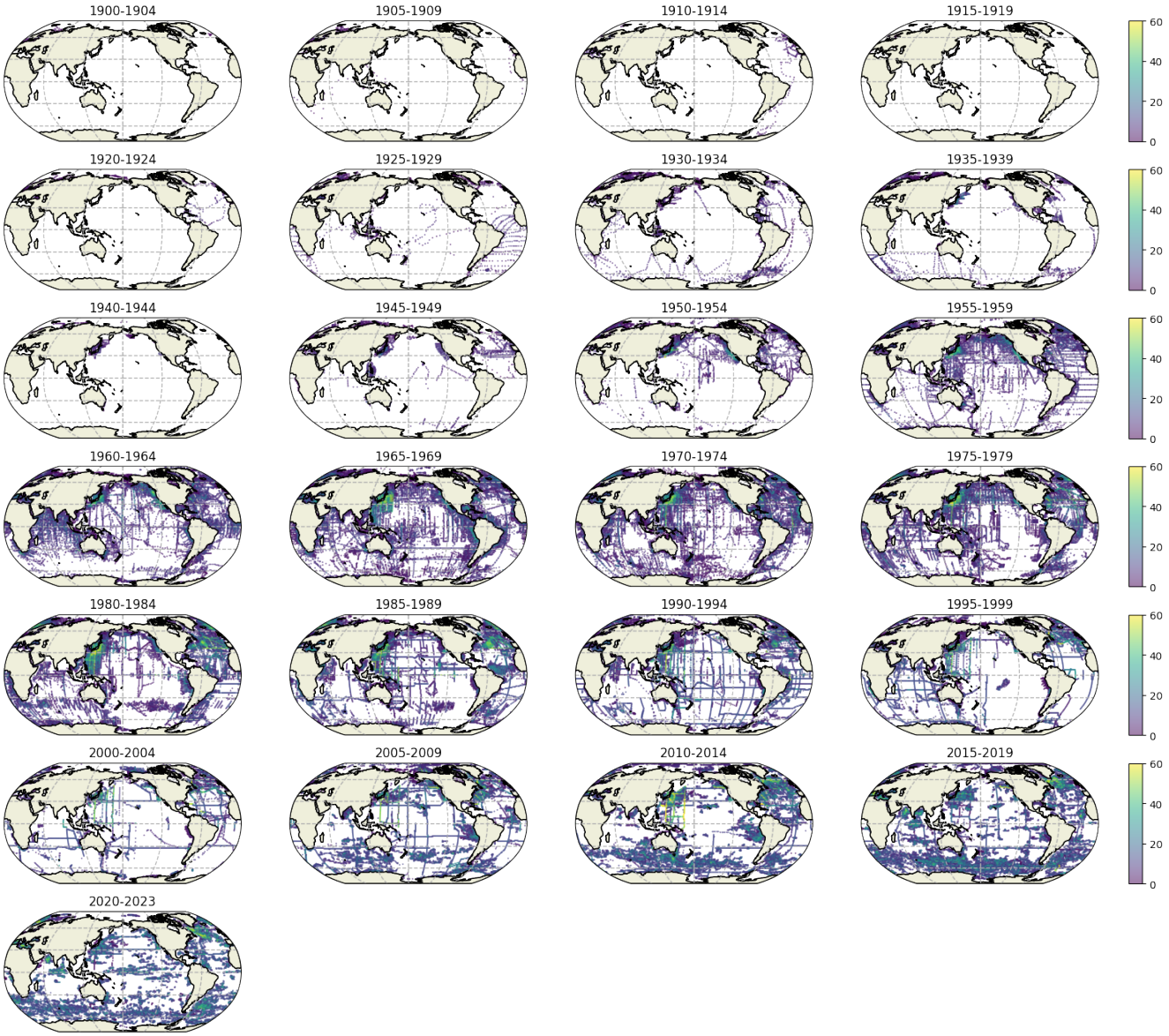

Figure S1. Spatial distribution of dissolved oxygen gridded data every five years. The color bar displays the proportion (%) of available observed data for each grid. The gridded data shows significant sparse and uneven distribution. There was a noticeable increase in data volume after 1955-1959. Therefore, our study primarily focuses on the period after 1960.

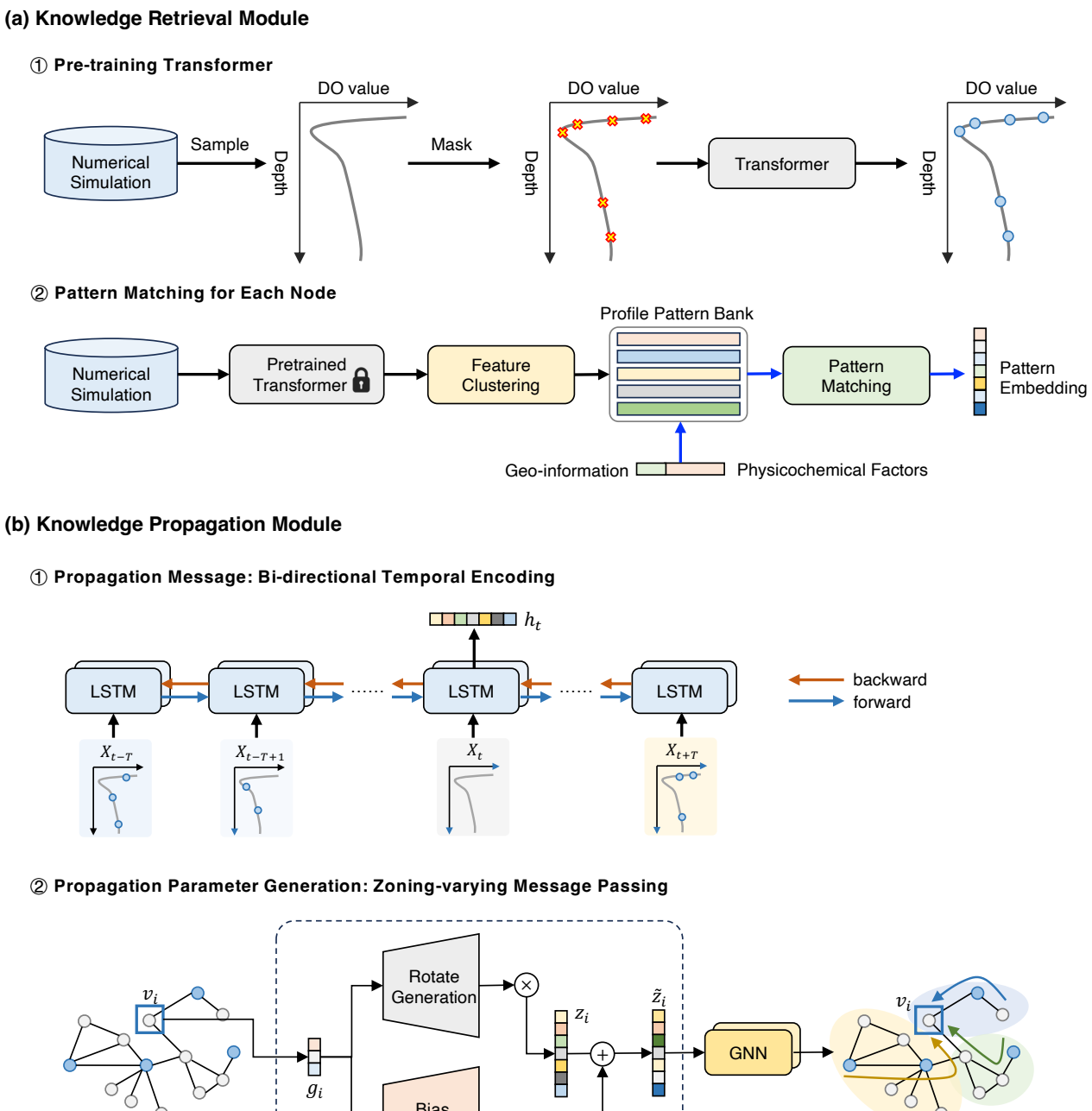

Figure S2. Module design details of Jingwei. a, Knowledge Retrieval Module. This module is further divided into two steps: first, pre-training the Transformer model using CMIP6 model data; second, obtaining a pattern bank and using node-level environmental variables as queries to retrieve pattern embeddings. **b**, Knowledge Propagation Module. First, bidirectional temporal encoding is performed using LSTM to derive temporal patterns at time t based on historical T steps and future T steps of temporal observation data. Second, an affine transformation (including rotation and bias) parameter is generated to the propagation information of the graph neural network, enabling zoning-varying message passing.

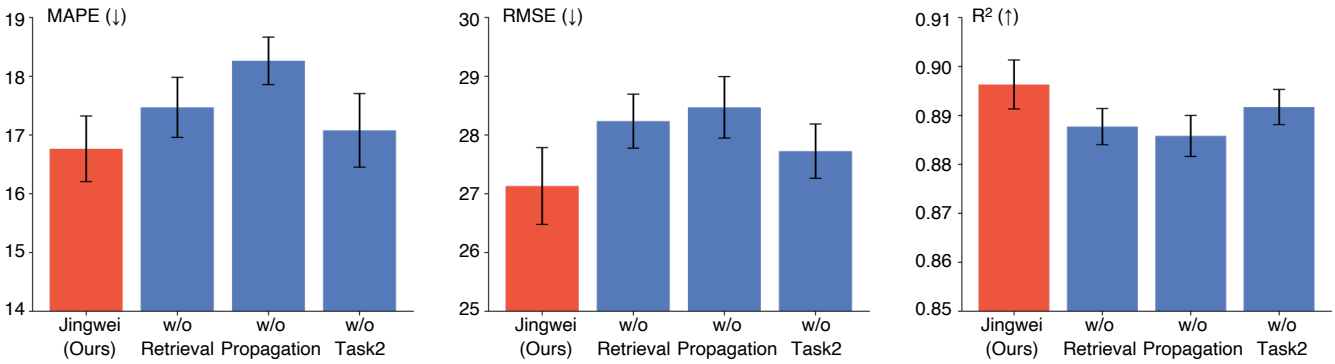

Figure S3. Ablation study of Jingwei. In the context of Jingwei framework, we analyze the impact of removing Knowledge Retrieval Module, Knowledge Propagation Module, and Task 2 Supervision (Self-supervised geo-coordinate regression) measured by MAPE, RMSE, and R^2. Our findings indicate that the removal of any individual module significantly affects model performance. Overall, Knowledge Propagation has the most substantial impact, followed by Knowledge Retrieval.

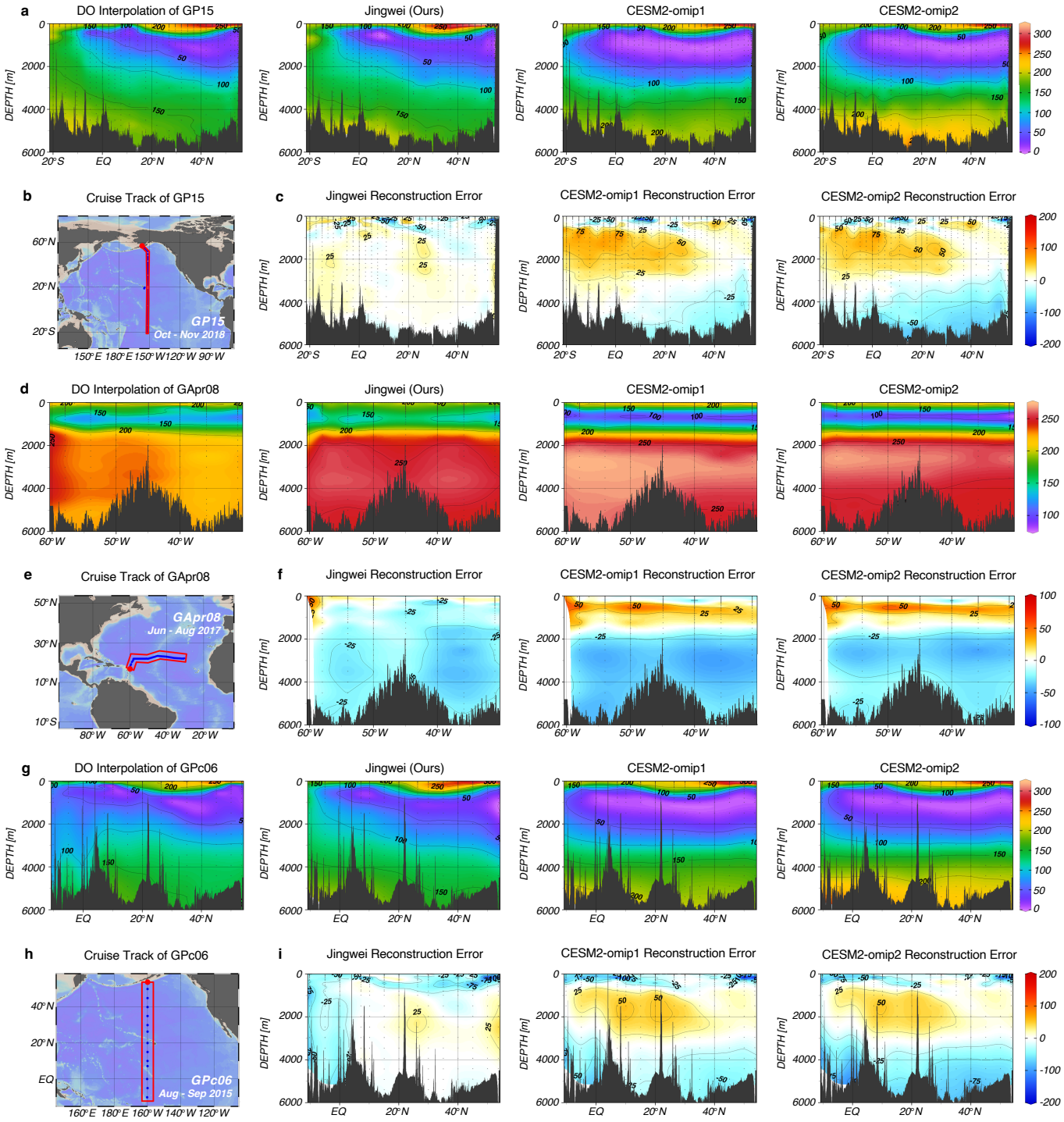

Figure S4. Dense observations and reconstruction comparison of dissolved oxygen in cruise GP15, GApr08, GPc06. b, e, h, Geographical location information for three cruises. **a, d, g**, The interpolation results of dissolved oxygen obtained from dense observations (considered as ground truth), and results from Jingwei, CESM-omip1, and CESM-omip2. The simulations from GFDL-ESM4 are excluded from the comparison, as they only extend until 2014. **c, f, i**, The errors between different methods and the ground truth, revealing that Jingwei achieves the optimal reconstruction performance.

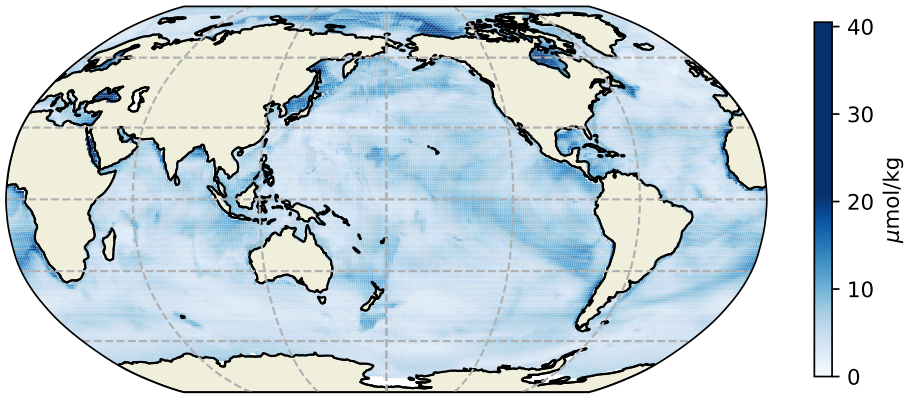

Figure S5. The uncertainty of Jingwei model reconstruction. The global overall uncertainty of Jingwei is 6.410 μmol/kg. In the Arctic region, due to the relatively low number of observations, a higher uncertainty is observed. Additionally, in the coastal areas, the influence of human activities makes accurate predictions more challenging, resulting in Jingwei also indicating larger uncertainty than in other regions.

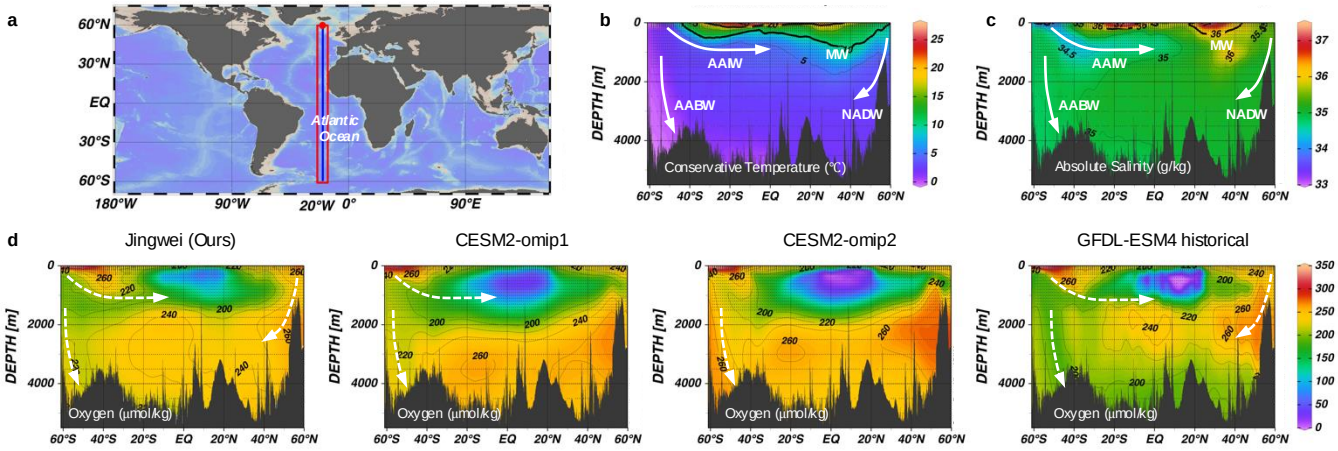

Figure S6. Reconstruction performance of Atlantic Meridional Overturning Circulation (AMOC). AMOC is a circulation system that integrates surface and deep currents in the Atlantic, with a generally stable overall pattern. The variation in dissolved oxygen concentration is influenced by the movement of AMOC water masses. **a**, We select the 20°W to observe the changes in dissolved oxygen concentration along this section. **b, c**, The distribution of conservative temperature and absolute salinity based on temperature and salinity observations, showing the variations of several AMOC water masses (AAIW, MW, AABW, and NADW). **d**, Comparison of the temporal average dissolved oxygen concentration distributions between Jingwei and three simulation results, i.e., CESM2-OMIP1, CESM2-OMIP2, and GFDL-ESM4, which reveals that Jingwei's reconstruction results effectively reflect the impact of various AMOC water masses on dissolved oxygen. This confirms that our data-driven reconstruction aligns with oceanographic principles and further demonstrates the effectiveness of our proposed method.

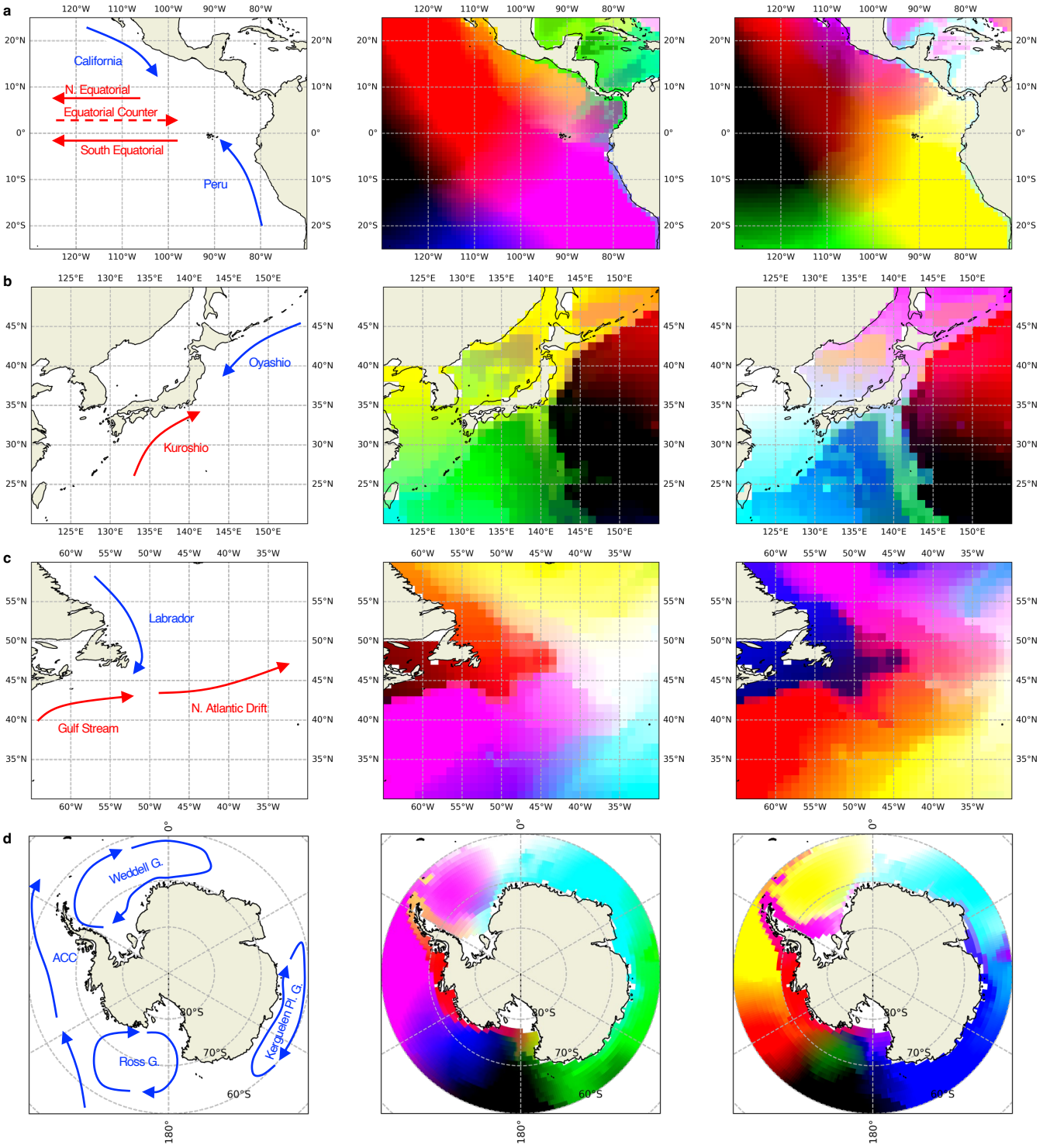

Figure S7. More cases on Jingwei's spatial heterogeneity perception ability. a, Eastern Equatorial Pacific: The regions traversed by the California Current and the Peru Current exhibit differences, with spatial features gradually changing as the offshore distance increases. **b**, Northwest Pacific, east of Japan: The regions traversed by the Oyashio Current and the Kuroshio Current exhibit differences, with the partition boundaries extending southeastward. **c**, Northwest Atlantic, east of Canada: The regions traversed by the Labrador Current and the Gulf Stream exhibit differences, with the junction evolving different features of the North Atlantic Drift further east. **d**, Southern Ocean: The presence of gyres in the Ross Sea, Weddell Sea, and Kerguelen Plateau, along with other factors, results in uniform internal features that distinguish these regions from surrounding waters.

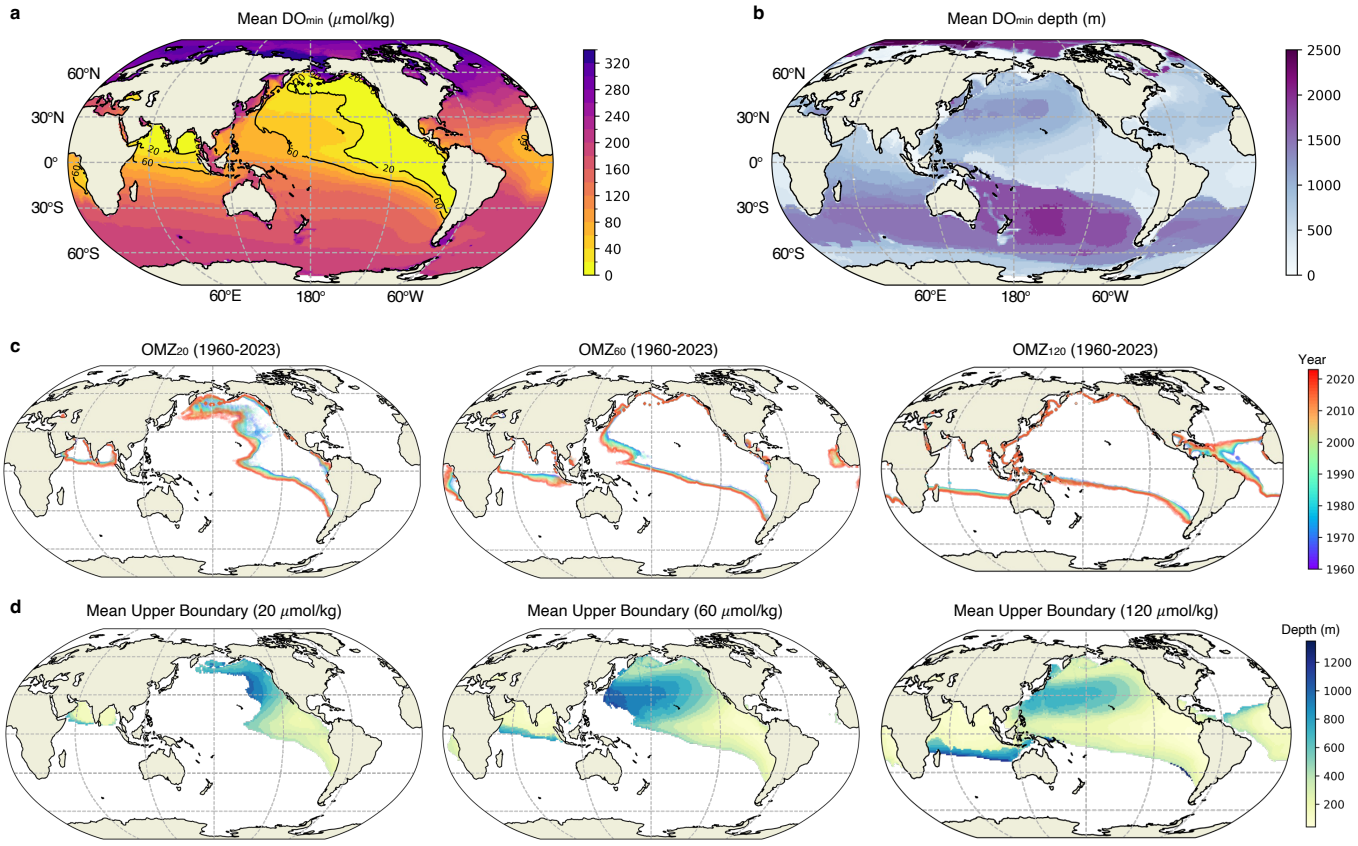

Figure S8. Horizontal and vertical distribution of oxygen minimum zones (OMZs). a, The average of the minimum dissolved oxygen concentration (DO_{min}) within each profile. The map also shows the average ranges of areas where DO_{min} below 20 μmol/kg (OMZ_{20}, solid line) and DO_{min} below 60 μmol/kg (OMZ_{60}, dashed line). The distribution of OMZs exhibits a significant north-south asymmetry, concentrated in the North Indian Ocean, the North Pacific, and the Equatorial Pacific. **b**, The average of DO_{min} depth. **c**, Annual changes in the horizontal distribution of OMZ_{20}, OMZ_{60} and OMZ_{120} from 1960 to 2023. OMZs present a trend of expansion in most regions. **d**, The mean depth of upper boundary for OMZ_{20}, OMZ_{60} and OMZ_{120}. The upper boundary of OMZs in the Indian Ocean deepens from north to south, whereas in the Pacific Ocean, OMZs deepen westward and northward from the equatorial region, before becoming shallower again near 50°N.

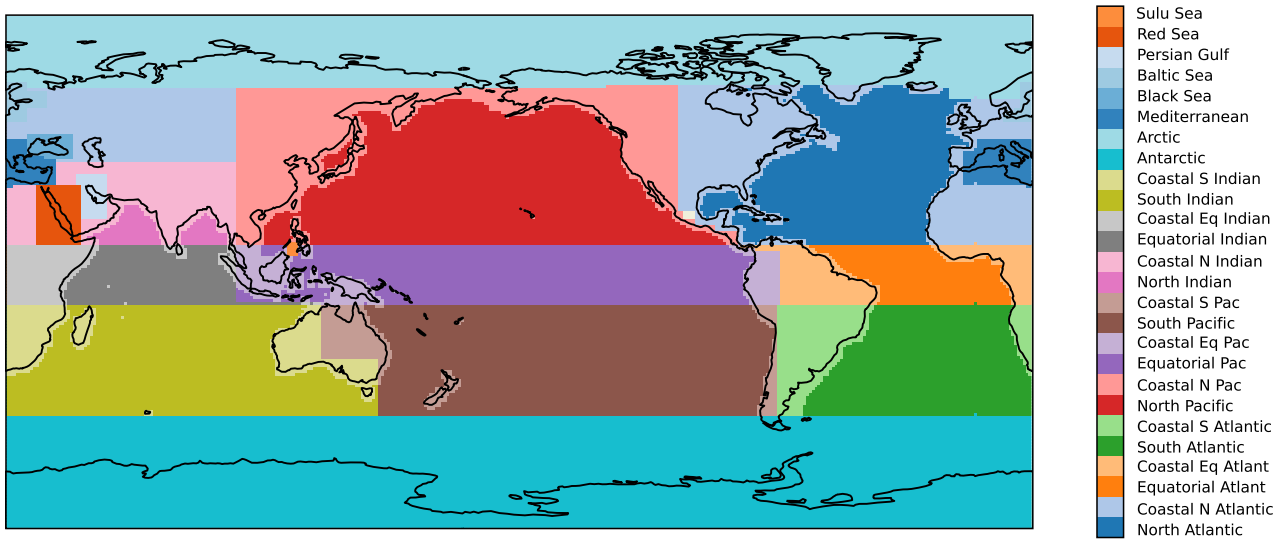

Figure S9. Geographic boundaries of ocean basin definitions in WOD18. World Ocean Database 2018 (WOD18) divides the world's oceans into 26 different zones based on hand-crafted rules. The zoning strategy for WOD mainly relies on ocean basins. Ocean basins are the basic geographic units of the global oceans, which indicate large bodies of water consisting of oceanic ridges, continental slopes and ocean basins. Ocean basin zoning aims to divide the global ocean into major regions according to different geographic, geological, and oceanographic features.

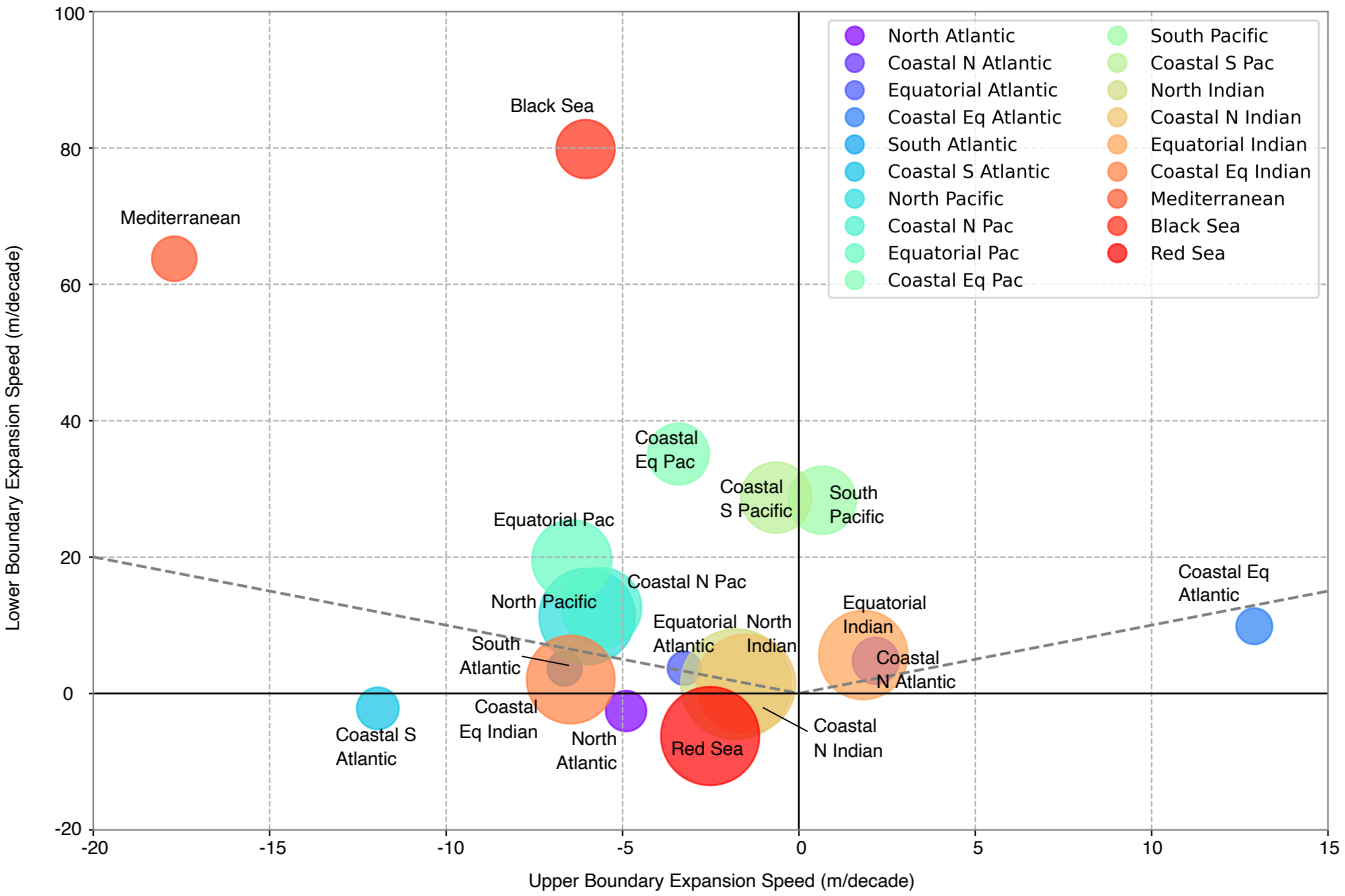

Figure S10. Vertical expansion of OMZ_{60}, i.e., hypoxic waters, in different ocean areas. The horizontal and vertical axes represent the expansion rates of the upper and lower boundaries, respectively. The size of each point indicates the average thickness of the OMZ. A negative expansion speed of the boundary indicates an upward movement of the boundary, while a positive speed indicates a downward movement.

Figure S11. The logo design of Jingwei. The central theme depicts the mythical bird Jingwei blending with ocean waves, with Jingwei holding in its beak a 'digital branch' symbolizing data flow.

Table S1. Detailed Information of data sources for global ocean observations.

Database	Time	Institution	Source	Access Date
World Ocean Database (WOD 2018)	1900-2023	National Centers for Environmental Information	https://www.ncei.noaa.gov/	2023-05
CLIVAR and Carbon Hydrographic Database (CCHDO)	1922-2023	CLIVAR and Carbon Hydrographic Data Office	https://cchdo.ucsd.edu/	2023-05
Argo	2001-2023	Argo Global Data Assembly Center	https://argo.ucsd.edu/	2023-05
Global Ocean Data Analysis Project version2.2022 (GLODAPV2_2022)	1972-2021	NOAA's National Centers for Environmental Information (NCEI)	https://glodap.info/	2023-05
Geotraces IDP	2007-2018	GEOTRACES International Data Assembly Centre (GDAC)	https://www.geotraces.org	2023-10

Table S2. Flag system of multiple databases.

FLAG	WOD	CCHDO	Argo	GLODAPV2_2022	IDP 2021
0: good quality	0	2	1	2	1
1: unknown quality	N/A	0,1,5,8	N/A	N/A	0,5
2: questionable quality	1	3,6,7	2,3	0	2,3,6,7,8,A,B,Q
3: bad quality	2,3,4,5,6,7,8,9	4	4	N/A	4
4: not sampled	N/A	9	0,5	9	9

Table S3. Detailed Information of Simulation Data from CMIP6.

Model	Experiment	Institution	Access Date
Community Earth System Model (CESM2)[12]	omip1	National Center for Atmospheric Research (NCAR)	2023-11
Community Earth System Model (CESM2)[12]	omip2	National Center for Atmospheric Research (NCAR)	2023-11
Geophysical Fluid Dynamics Laboratory - Earth System Model (GFDL-ESM4)[13]	historical	NOAA's Geophysical Fluid Dynamics Laboratory (GFDL)	2023-11

Table S5. Dividing the ocean from the surface to 5,500 meters into 33 depth layers.

Layer ID	Depth Level (m)	Level Boundary (m)	
1	0	0	5
2	10	5	15
3	20	15	25
4	30	25	40
5	50	40	62.5
6	75	62.5	87.5
7	100	87.5	112.5
8	125	112.5	137.5
9	150	137.5	175
10	200	175	225
11	250	225	275
12	300	275	350
13	400	350	450
14	500	450	550
15	600	550	650
16	700	650	750
17	800	750	850
18	900	850	950
19	1000	950	1050
20	1100	1050	1150
21	1200	1150	1250
22	1300	1250	1350
23	1400	1350	1450
24	1500	1450	1625
25	1750	1625	1875
26	2000	1875	2250
27	2500	2250	2750
28	3000	2750	3250
29	3500	3250	3750
30	4000	3750	4250
31	4500	4250	4750
32	5000	4750	5250
33	5500	5250	5500

Table S4. Predictor variables used to train Jingwei. Unitless quantities are denoted using '-'.

Predictor Variable	Abbreviation	Unit	Range (approx.)
Dissolved oxygen (simulated data)	D_{sim}	μmol/kg	-10 to 405
Dissolved oxygen (observation data)	D_{obs}	μmol/kg	0 to 509
DO observation at time τ	X_τ	μmol/kg	0 to 509
Conservative temperature	T	°C	-3 to 34
Absolute salinity	S	PSU	0 to 41
Seawater density	ρ	kg/m^3	995 to 1055
Seawater pressure	P	dbar	0 to 5617
Latitude	lat	-	-90 to 90
Longitude	lon	-	-180 to 180
Spheroidal coordinates	x, y, z	-	0 to 1
Depth	L	m	0 to 5500
Year	yr	year	1960 to 2023
Bathymetry	L_b	m	-8000 to 5500

Table S6. Mean oxygen content based on Jingwei and comparison with the results from Nature'17[1]. Based on the global ocean partition in Nature'17, we calculate the mean oxygen content globally and in different regions using the oxygen levels reconstructed by Jingwei. The results from both approaches are generally consistent and mutually validate that the existing estimates of the total ocean oxygen inventory are accurate. However, there are certain discrepancies in the understanding of specific regions. For instance, the total oxygen levels in the equatorial regions (Equatorial Atlantic, Equatorial Pacific, and Equatorial Indian Ocean) are underestimated, while those in the North Pacific, South Pacific, and South Indian Ocean are overestimated.

Oxygen Content (Pmol)	Nature'17[1]	Jingwei (Ours)	Mean Diff.	Diff. Ratio
Arctic Ocean	4.73±0.16	5.42±0.04	0.69	14.68%
North Atlantic	26.86±0.05	29.02±0.08	2.16	8.04%
Eq. Atlantic	15.89±0.04	11.13±0.02	-4.76	-29.94%
South Atlantic	22.39±0.05	24.44±0.04	2.05	9.16%
North Pacific	24.48±0.10	29.77±0.06	5.29	21.60%
Eq. Pacific	25.49±0.40	19.52±0.14	-5.97	-23.42%
South Pacific	33.05±0.07	36.73±0.04	3.68	11.14%
Eq. Indian Ocean	10.74±0.08	7.21±0.02	-3.53	-32.86%
South Indian Ocean	26.13±0.06	29.95±0.02	3.82	14.61%
Southern Ocean	37.62±0.09	37.06±0.07	-0.56	-1.48%
Total	227.38±1.10	232.13±0.20	4.75	2.09%
Total (0-1200 m)	62.26±0.43	67.45±0.10	5.19	8.34%
Total (1200 m – bottom)	165.12±0.67	164.68±0.17	-0.44	-0.27%

Table S7. Vertical expansion speed and thickness of hypoxic zones in various ocean regions around the world.

Regions	OMZ_{20} ($O_2 \leq 20\mu$mol/kg)			OMZ_{60} ($O_2 \leq 60\mu$mol/kg)		
	Upper Boundary (m/dec)	Lower Boundary (m/dec)	Avg. OMZ Thickness (m)	Upper Boundary (m/dec)	Lower Boundary (m/dec)	Avg. OMZ Thickness (m)
North Atlantic	-	-	-	-4.899	-2.581	162.055
Coastal N Atlantic	-	-	-	2.177	4.804	211.229
Equatorial Atlantic	-	-	-	-3.246	3.683	110.422
Coastal Eq Atlantic	-	-	-	12.906	9.873	128.881
South Atlantic	-	-	-	-6.645	3.666	116.926
Coastal S Atlantic	-	-	-	-11.936	-2.193	173.867
North Pacific	-3.256	9.566	400.193	-6.003	11.291	900.679
Coastal N Pac	-5.362	5.729	311.617	-5.586	12.600	616.966
Equatorial Pac	-8.046	7.995	306.746	-6.433	19.591	623.500
Coastal Eq Pac	10.778	9.841	257.929	-3.415	35.110	369.667
South Pacific	-0.708	8.323	213.959	0.667	28.338	449.600
Coastal S Pac	0.166	7.647	233.206	-0.646	28.726	489.382
North Indian	-9.310	16.583	680.934	-1.779	1.362	1192.305
Coastal N Indian	-11.883	15.266	595.806	-1.507	1.396	968.612
Equatorial Indian	-3.941	14.691	373.988	1.829	5.628	774.849
Coastal Eq Indian	-8.518	1.173	420.885	-6.467	2.025	761.019
Mediterranean	-	-	-	-17.708	63.748	197.267
Black Sea	1.094E-14	3.668E-15	37.500	-6.044	79.838	336.777
Red Sea	-	-	-	-2.517	-6.245	949.961